STRUCTURE OF ZIRCALOY-4 OXIDES FORMED DURING AUTOCLAVE CORROSION

Benoit de Gabory and Arthur T. Motta

Department of Mechanical and Nuclear Engineering, The Pennsylvania State University,
227 Reber Building, University Park, PA 16802 - bml192@psu.edu

The extent of waterside corrosion of zirconium alloy fuel cladding is a strong function of the specific alloy used. To rationalize the details of the corrosion kinetics obtained during autoclave corrosion of alloys, a Transmission Electron Microscope (TEM) study of Zircaloy-4 oxide structures is performed at various stages of corrosion. Using focused ion beam (FIB), TEM samples were lifted out of the oxide layer at precise locations in the oxide, or near the oxide/metal interface. The study characterizes the oxide grain size and morphology, oxide texture, incorporation of metallic precipitates and the evolution of these with respect to the distance to the oxide/metal interface. Special attention was given to the oxide-metal interface to determine the phases present, and measure the evolution of oxygen content in the oxide precursor layers. Results show that the oxide is mainly monoclinic, with a small fraction of tetragonal phase, with a preponderance of columnar oxide grains, which extend to the oxide metal interface. The interface exhibits both an intermediate layer and a discontinuous layer of "blocky" grains on the metal matrix side, which change upon transition and which could be identified with suboxide phases, corresponding to a level of higher oxygen content.

I. INTRODUCTION

Zirconium-based alloys are widely used in the nuclear industry, because of their good mechanical behavior, resistance to corrosion, and low thermal neutron absorption cross-section. Although Zircaloy-4 has been used for the past sixty years, its corrosion behavior is still under investigation, as a more complete understanding of its corrosion kinetics can help to design better alloys.

The different corrosion rates observed in different alloys are thought to be related to the microstructure of the respective oxide layers formed in these alloys. In his context, a detailed characterization of this structure and interface between oxide and metal is key to developing an understanding for alloy improvement.

Zircaloy-4 recrystallized sheet samples were autoclave corroded in 360°C water at saturation pressure at Westinghouse Electric Company. Fig. 1 shows the oxidation kinetics, determined by measuring weight gain. The periodic behavior characteristic of the corrosion of Zircaloy-4 is observed, with two marked transitions clearly visible. Coupon samples were archived at different corrosion times for examination. The three samples selected were from just before and just after the first oxide transition, as indicated by the arrows in Fig. 1.

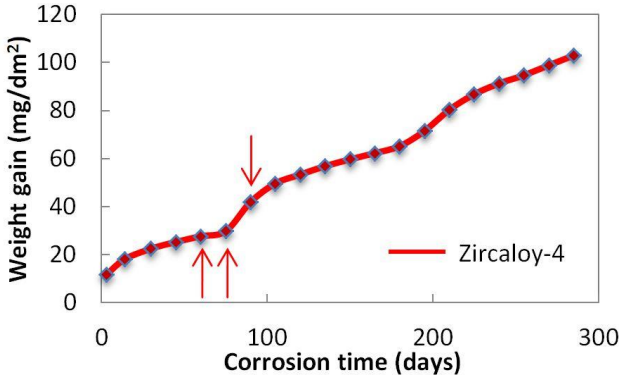

Fig. 1: Corrosion weight gain versus exposure time in 360°C water; studied samples are arrowed.

II. EXPERIMENTAL METHODS

The Zircaloy-4 oxide samples selected were made into cross-sectional specimens by grinding and polishing. From these, TEM samples were prepared using the FIB in-situ lift-out technique. The instrument, a FEI Quanta 3D 200, was operated at 30keV, with currents between 30 pA and 7.0 nA. The lift out method consists of extracting a thin foil from the sample, attaching it to a copper grid, and thinning it down even more to reach electron transparency (~ 100 nm thickness). This technique provides homogeneously-thinned TEM samples, taken from precise locations, e.g. close to the oxide/metal interface (OMI) and with large transparent areas to study. From each Zircaloy oxide sample many such foils were extracted, so that detailed information could be obtained.

For examination, a JEOL 2010 TEM and a JEOL 2010F Scanning Transmission Electron Microscope (STEM) – for Electron Energy Loss Spectroscopy (EELS) measurements – were used at the Materials

Characterization Laboratory at Penn State. These microscopes operate at 200keV and are both equipped with a Gatan GIF spectrometer.

III. EXPERIMENTAL RESULTS

III.A. Oxide morphology

The three samples studied– pre- and post-transition – have a thickness of the oxide in the 2-3 micron range. The α-Zr phase metal grains are equiaxed with a diameter between 1 and 3 microns. In the hcp matrix near the oxide/metal interface, hydrides are often observed, as well as unoxidized second phase particles (SPP) of the type $Zr(Fe,Cr)_2$.

In the oxide, both large columnar grains and smaller equiaxed grains were observed. The latter are more prevalent near the oxide/water interface and in the regions surrounding cracks. SPP are found either unoxidized and crystalline, or oxidized in the form of small grains. Large lateral cracks are found mainly parallel to the oxide metal interface. Although these cracks are believed to be created during sample preparation, they are an indication of weaker points in the structure of the oxide[1], usually found in regions containing equiaxed grains as seen in (Fig. 1).

The sizes of the two different grain morphologies have been measured. Columnar grains are quite elongated, measuring about 80-300 nm long and 10-40 nm wide. The averages are around 140 and 20 nm, respectively. The aspect ratio (length/width) remains within the 4-12 range, with an average value of 7. As a general rule, the longer the grains, the wider they are. Equiaxed grains have a diameter between 10 and 25 nm, a size comparable to the columnar grain width. In the post-transition sample, by calculating the weight gain since the transition (14.7 mg/dm^2 ↔ 1 micron) and taking that distance from the oxide metal interface the place where the transition took place can be found. This location turns out to exhibit a layer of equiaxed grains (Fig. 2).

The oxide grown after the transition exhibits a similar structure as the one grown at the start of the corrosion. The only difference is a slight decrease in the grain length for the first hundreds of nanometers after the transition.

The structure of the oxide is more clearly shown in Fig. 2. Detailed observation of the micrographs in the upper picture allowed to create a tracing designed to make the morphology appear more clearly. As shown, most of the oxide layer is constituted of long columnar grains, aligned in the oxide growth direction and perpendicular to the oxide/metal interface. A layer of equiaxed grains can be seen ~ 800 nm away from the interface. This length corresponds to the oxide growth since transition, as calculated from the weight gain curve (Fig. 1). Two large cracks can be seen going through that layer, as well as smaller ones.

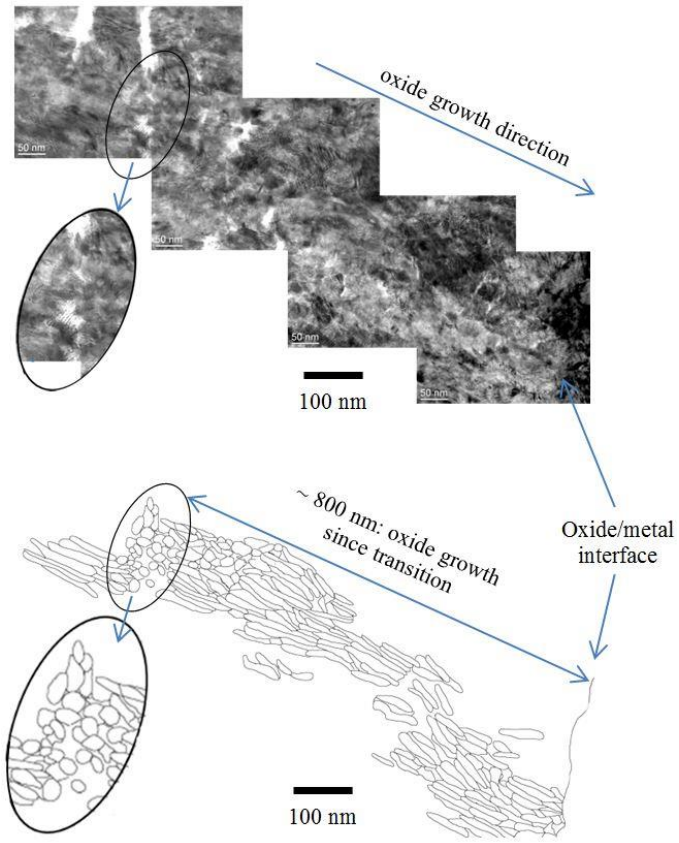

Fig. 2: Morphology of the oxide grown after transition

The columnar grains above each react differently to tilt, a consequence of the strong grain-to-grain misorientation, as observed before[1].

III.B. Oxide texture

Both monoclinic and tetragonal ZrO_2 phases are found in the oxide layer: the stable monoclinic phase and the metastable tetragonal phase, which is stabilized at the oxide formation temperature by alloying elements in solid solution, small grains and high compressive stresses – conditions that are reunited in the oxide layer, especially near the oxide/metal interface.

The crystallographic texture of the oxide layer has been studied at different positions using electron diffraction. A large selected area aperture (~100 nm in diameter) has been used. This area contains many oxide grains, which explains the rings observed in the diffraction patterns that were taken, but also gives us representative data for our texture analysis.

A diffraction pattern analysis was performed as was done by Yilmazbayhan[1]. Mainly monoclinic reflections can be seen, with the exception of the $(101)_T$ peak. The intensity of the reflections varies along the ring, allowing us to draw some conclusions as to the crystallographic orientation of the grains in this layer.

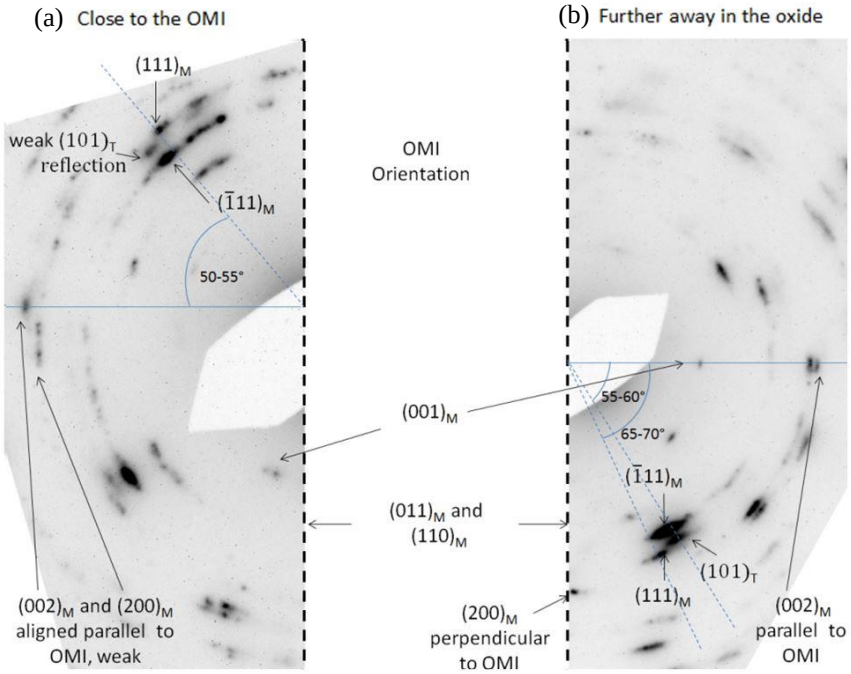

Fig. 3: Electron diffraction patterns taken from areas (a) close to the oxide/metal interface and (b) in the bulk of the oxide

The tetragonal $(101)_T$ peak reflection is usually stronger close to the oxide/metal interface. In the pattern presented in Fig. 3, it is seen to be stronger far from the interface than close to it because it was taken in the post-transition oxide, in a region encompassing the equiaxed grains studied above. This would tend to confirm the presence of tetragonal zirconia observed in the small grains formed at transition[1]. The alignment of this reflection is similar to the $(111)_M$ and $(\bar{1}11)_M$: about 50-70° from the oxide surface normal.

These two peaks are very often aligned, with the $(101)_T$ in between them. There are variations in intensity along their diffraction rings, with peaks around 60-70° for the $(111)_M$ and 50-60° for the $(\bar{1}11)_M$. These results confirm those obtained by X-Ray diffraction by Bechade et al[2].

More information on the oxide texture can also be obtained from the $(200)_M$, $(020)_M$ and $(002)_M$ peaks. Although the $(200)_M$ and $(020)_M$ reflections are close in d-spacing and difficult to distinguish, previous synchrotron studies[3] identified the peaks found at this location as $(200)_M$. Near the oxide/metal interface, both $(002)_M$ and $(200)_M$ reflections are weak and more or less aligned parallel to the interface. Further into the bulk of the oxide, the reflections are more localized, indicating a preferential orientation, parallel to the interface for $(002)_M$, and close to the oxide growth direction for the $(200)_M$.

The observations confirm that the texture of the oxide is better defined as we move further away from the oxide/metal interface. Similar diffractions patterns have been taken at different positions along the interface, and in different samples (pre-and post-transition), yielding similar results.

III.C. Second phase particles

Second phase particles (SPP) are found in Zircaloy-4 in the form of $Zr(Fe,Cr)_2$ precipitates. These are often faceted, with a diameter between 100 and 200 nm, and are found unoxidized in the metal. When incorporated into the oxide layer, they are found either in their unoxidized state when near the oxide/metal interface (Fig. 4) or later oxidized in the oxide matrix[4] (Fig. 5).

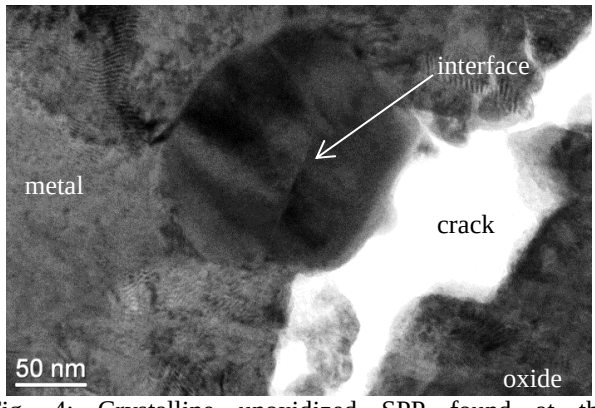

Fig. 4: Crystalline unoxidized SPP found at the oxide/metal interface

Stacking faults can often be seen in the crystalline precipitates. For the incorporated SPP, a crack is often observed on the side of the precipitate opposite to the

interface. The presence of this crack can be explained by two factors: the delayed oxidation of the SPP, and the volume expansion of the matrix when it becomes oxidized: while the precipitate remains unoxidized (and its volume does not change), the matrix around it keeps oxidizing and expanding in the oxide growth direction. This leads to the formation of a crack on top of the precipitates.

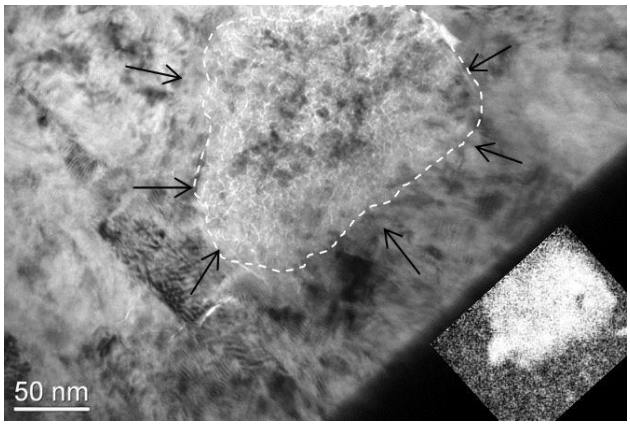

Fig. 5: Arrows indicate an oxidized precipitate. In the box, a Fe EFTEM map confirms its localization.

Oxidized precipitates are not as easy to observe as unoxidized ones. These have been found in the oxide at distances as close as 300 nm from the oxide interface (a distance at which crystalline SPP can still be observed as well). In bright field imaging, they appear as a round/oval collection of small equiaxed grains with a diameter on the order of 10 nm, separated by small cracks (see Fig. 5). An Energy Filter TEM (EFTEM) mapping of the oxide for both Cr and Fe (the Fe map is shown in the box, Fig. 5) shows a high concentration of these elements in the dissolved precipitate, and, to a smaller measure, in the oxide surrounding it.

A diffraction pattern taken from the oxidized SPP shows a higher intensity of tetragonal oxide peaks, which is in agreement with small equiaxed grains being associated with the tetragonal phase. The stabilization of the tetragonal phase can be explained by the high concentration of alloying elements and the stresses due to the delayed volume expansion of the precipitate compared to the oxide matrix.

III.D. Oxide/metal interface

The oxide/metal interface has been the focus of many studies, because this is the region where new oxide grains are formed and, as such, it impacts the structure of the oxide and the properties of the alloy; and yet its structure is not well known.

Although the interface is not always easy to identify, EFTEM oxygen maps can help position it accurately.

Between the newly formed oxide grains and the metal, bright field pictures show a thin intermediate layer in samples from both before and after transition. The thickness of this layer varies from sample to sample, between 10 (after transition) and 60 nm (before transition).

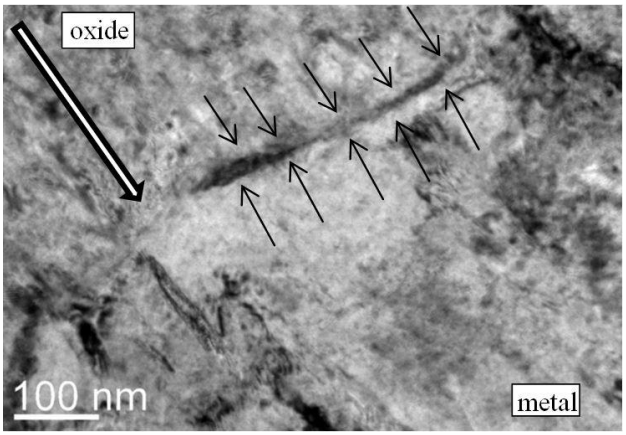

Fig. 6: The intermediate layer in a post-transition oxide. Oxide growth direction is indicated by the large arrow.

In some places along the oxide/metal interface, some blocky grains can be seen, interrupting the continuity of the intermediate layer[1]. These are arrowed and appear as dark features in Fig. 7. Using electron diffraction, these have been identified as rhombohedral Zr_3O.

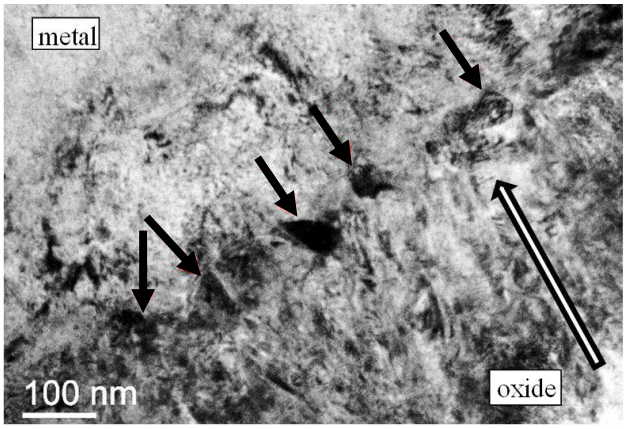

Fig. 7: Blocky grains indicated by the dark arrows. The long arrow is oriented in the oxide growth direction.

In the pre-transition sample, close to the transition, the region in the metal near the interface exhibits a different color and reaction to tilting than the metal grain. This region is about 250 nm wide (see Fig. 8). An electron diffraction pattern taken in order to identify this structure has been indexed as ω-Zr (Fig. 8), a metastable hexagonal phase that has been previously observed in several alloys of Zr and Ti[5]. The α->ω transformation is induced by the application of significant pressure (of the order of 1-10 GPa).

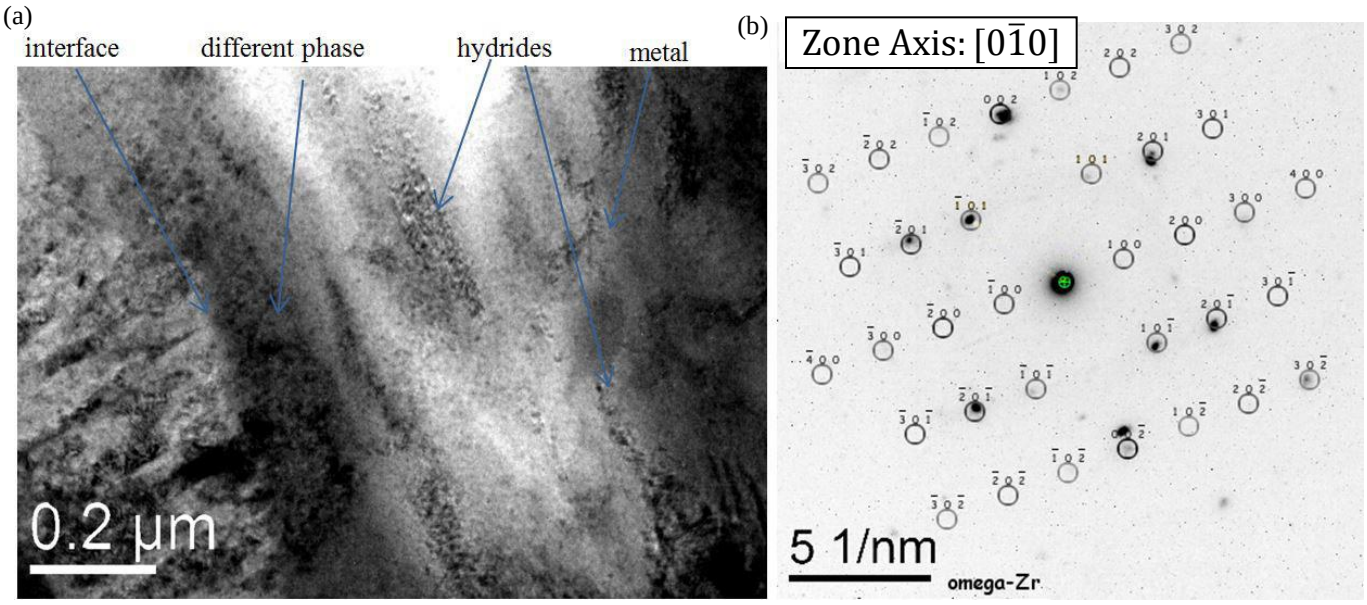

Fig. 8: (a) The phase present between the metal and the oxide. (b) Diffraction pattern taken from this region, indexed as ω-Zr.

Another way to study the oxide/metal interface is to measure via Electron Energy Loss Spectroscopy (EELS) the evolution of the oxygen content across the oxide/metal interface. For these scans, a probe size of 1.0 nm, a camera length of 8 cm and an aperture of 2 mm were used, with steps of 1.5 nm. The edges of interest are the Zr $M_{4,5}$-edge at 180 eV and the O K-edge at 530 eV.

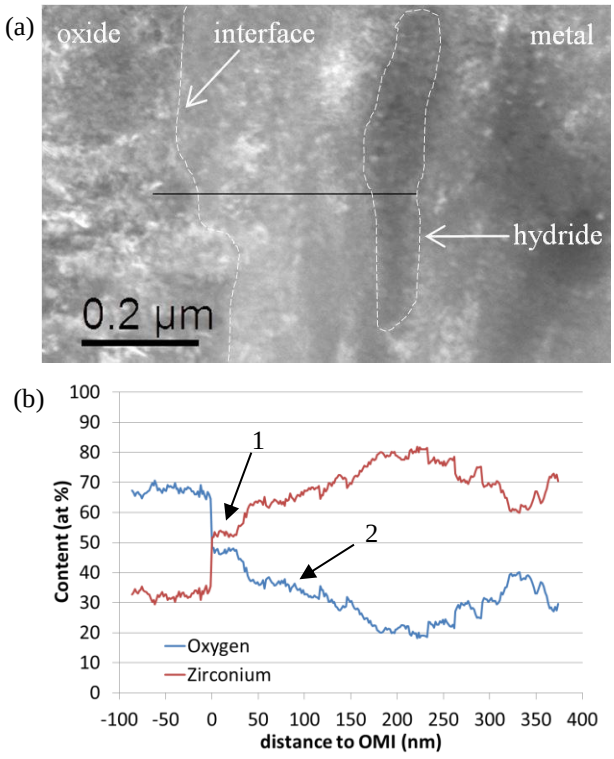

Fig. 9: (a) High Angle Annular Dark Field (HAADF) picture and (b) EELS signal in pre-transition oxide.

Using the STEM, High Angle Annular Dark Field pictures were obtained. This technique gives better mass-contract than bright field imaging. From those pictures, EELS line scans were taken across the oxide/metal interface, allowing the determination of the oxygen content. They all have features in common: a more or less flat line at 66 O at% in the oxide, then a decrease at the oxide/metal interface, until around 30 O at% – limit solid solubility of oxygen in the α-Zr – and finally a decrease deeper into the metal. However, there are significant differences between pre-transition oxides close to the transition and post-transition oxides.

For the pre-transition oxide, a thick layer after the oxide shows a high O content (100 nm layer at around 30 at% indicated by arrow (2) in Fig. 9). At the position indicated by the arrow (1) in Fig. 9, an intermediate layer about 40 nm wide with an approximate composition of 45 O at% can be seen in the metal. This value corresponds to the presence of a phase with a stoichiometry close to ZrO at the interface.

At the end of the scan, an increase in the oxygen content corresponds to the presence of a hydride. This result is probably due to the hydrogen in the hydride that could not be accounted for in the calculations.

The same pre-transition sample has also been studied using Atom Probe spectroscopy by Yan Dong and Emmanuelle Marquis at the University of Michigan[6]. This technique allows a very precise characterization of the oxygen content at the interface. The results are in agreement with and further develop the observations made in this study: after the oxide/metal interface, a first plateau (~ 40 nm wide) of composition 55 O at% is observed and associated with a ZrO_{1+x} phase. Then a second plateau, shorter (~15 nm), with an oxygen content

around 45 at%, is denoted ZrO_{1-x}. A plateau at 30 at% oxygen extends for 150 nm, before the O content decreases over 40 nm until it reaches its final value, around 4 at %.

The post-transition oxide does not exhibit such a thick oxygen-charged layer. When the limit solid solubility of O in the α-Zr matrix – around 30 O at% – is reached, there is no plateau at that value, but the O content quickly decreases so that at 100 nm away from the interface, there is less than 10 O at% remaining in the metal (see Fig. 10).

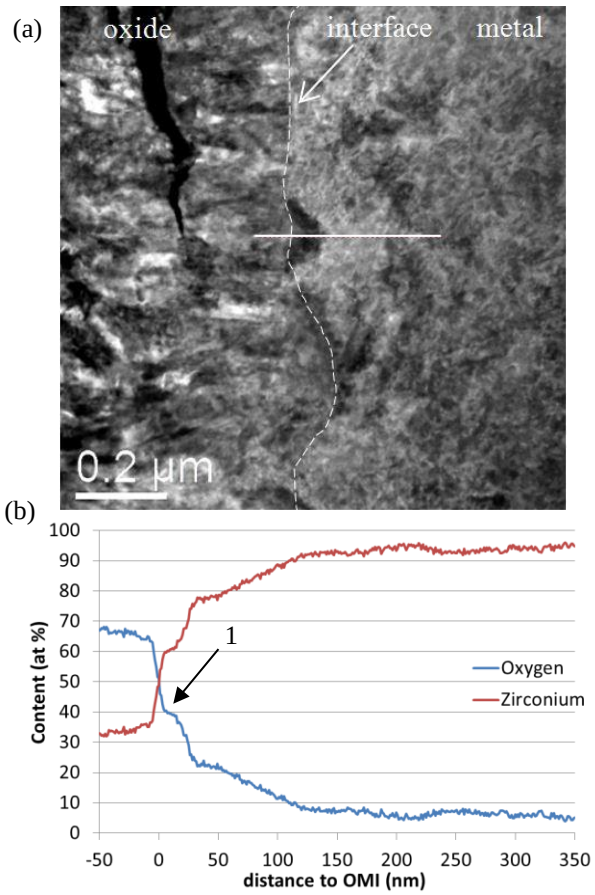

Fig. 10: (a) HAADF picture and (b) EELS signal in the post-transition oxide

A very small plateau 10 nm wide – indicated by the arrow (1) – is observed ahead of the oxide, containing about 40 O at%. Its width corresponds to the width of the intermediate layer observed in bright field (Fig. 6).

IV. DISCUSSION

The observations presented here are discussed and compared to previous TEM observations, and to results yielded by other characterization techniques, such as Atom Probe Tomography.

The Zircaloy-4 oxide exhibits an arrangement of mostly columnar grains with some small equiaxed grains. The equiaxed grains are mostly found close to the oxide water interface, near cracks, and, for post-transition samples, at the position where a transition took place. The columnar grains extend up to the oxide/metal interface. The texture studies show that the $(200)_M$ poles are aligned very close to the oxide growth direction, in good agreement with previous results[1]. The oxide texture is better defined far away from the interface, and more tetragonal signal can be seen in the areas containing equiaxed grains – since small grains are a factor of stabilization for the tetragonal phase at oxide formation temperature.

The explanation for those observations is that the oxide is initially formed as small equiaxed grains[7]. Some of these grains, correctly aligned to minimize stress, become columnar and keep growing as the interface advances into the metal. At transition, the oxidation rate increases quickly, leading to the rapid formation of small grains, some of which are not properly oriented to grow into columnar grains while minimizing stress accumulation. Thus the observation of the band of equiaxed grains at transition. Those grains have a higher grain boundary surface to volume ratio, making it easier for cracks to form to relieve the accumulated stress. Those cracks could also be created and/or enlarged by sample preparation – but they occur in regions that are conducive to their formation[1].

A higher grain boundary to volume ratio increases oxygen transport in the oxide, which is believed to occur by grain boundary diffusion[8]. It is thus difficult to conclude if the small equiaxed grains are a cause or an effect of transition (or both). It makes sense though, that larger and longer columnar grains are associated with slower corrosion kinetics. That also could explain why the high corrosion rate observed during the transition gradually decreases as the new protective layer grows: when longer grains are formed, the oxygen transport is slowed down, as well as the corrosion rate, as observed in Fig. 1.

The second phase particles (SPP) oxidize later than the matrix of Zircaloy-4. $Zr(Fe,Cr)_2$ precipitates can be seen unoxidized in the oxide matrix. A crack can be observed on top of them (opposite side of the oxide/metal interface). This is believed to be due to their delayed oxidation. The Pilling-Bedworth ratio of zirconium is 1.56. This means that, assuming the expansion is in the oxide growth direction, if the oxide/metal interface moves 1 nm into the metal, the position it was at has been "pushed" 0.56 nm away, and is now 1.56nm from the new interface. Since the SPP does not oxidize, there is no new grain formed, and on top of the precipitate, the oxide is still "pushed" by the surrounding matrix away from the surface of the SPP, creating the observed cracks.

Later (at a distance from the oxide/metal interface probably depending on its size), the precipitate becomes oxidized, forming small equiaxed grains. An electron

diffraction pattern shows that those grains are mainly tetragonal grains, once again stabilized by small grain size, the presence of alloying elements, and stresses created by the volume expansion of the precipitate in an enclosed space.

Although the interface has been the subject of much research, its morphology is not fully characterized. Both imaging and EELS oxygen content scans tend to show a broad variety of phases present at the interface. This variety also appears in the literature: Iltis and Michel[5] identified the ω-Zr phase in Zircaloy-4 by electron diffraction – with oxygen content around 25 at%. Foord and Newcomb[9] saw blocky grains at the oxide/metal interface of Zircaloy-4 samples and identified them as rhombohedral Zr_3O – a result confirmed by synchrotron studies[3]. Those blocky grains also have been sometimes identified as the ω phase. Finally, a ZrO cubic phase has been reported on a steam-oxidized Zircaloy[10]. The presence of this phase has been confirmed by Hutchinson[11] in Zircaloy-2 and Hudson[12] in zirconium.

Through imaging and by observing the reaction of the sample to tilting, an intermediate layer is clearly identifiable between the metal and the oxide: it is possible to get this layer to diffract strongly with neither the nearby oxide nor the metal in diffraction contrast (as seen in Fig. 6). The thickness of that layer varies between different samples: it increases continually until transition and becomes very small (~ 10 nm) after transition. One possible explanation is that this layer grows, then disappears at transition and starts to grow slowly again afterwards.

This intermediate layer is not consistently observed along the interface. In some places, no intermediate layer can be observed. In others, bigger blocky grains, strongly diffracting, are present at the interface. As these blocky grains are small, obtaining an electron diffraction pattern of those grains is no easy task, which could explain the discrepancies in the results presented above. The grains observed in this study were identified as Zr_3O. They are found in the pre-transition sample, and none could be observed after transition.

Before transition, a wide layer can be observed in the metal side of the interface, with a diffraction contrast differentiating it from the metal itself. This layer has been identified as the ω phase, a metastable phase of Zr formed by α->ω transformation which is triggered by high pressure.

Other ways to get information on the phases present at the interface and on the existence of a suboxide were investigated; one of them is to measure the evolution of the oxygen content across the interface, with fine spatial resolution (around 1 nm).

Many differences were observed in the microstructure of the interface between pre- and post-transition samples. Those differences also appear on the oxygen content curves we obtained by doing EELS scans across the interface.

For the pre-transition samples, a small plateau, 40 nm wide, at 45 O at% was observed. This plateau might be related to the intermediate layer that was observed earlier. A longer plateau at composition around 30 at% corresponds quite well to the different phase we observed in the metal side of the interface and identified as ω-Zr.

Those results are in broad agreement with the Atom Probe Tomography work done in the same sample[6]. This technique gives atomic resolution, but the TEM possesses two advantages: it is possible to study a large area (and thus a good length of the interface) while APT only gives results on a small needle (about 50 nm tip radius and 350 nm length); with a TEM, it is possible to relate the EELS results with imaging and electron diffraction results. Combining the two techniques is a powerful way of understanding oxide structure. As measured by Atom Probe Tomography, the intermediate layer is associated with some form of ZrO (and the two plateaus with ZrO_{1+x} and ZrO_{1-x}, two variations of this phase)

EELS scans run on one of the blocky grains revealed that the oxide content decreases from 30 at% to close to 5 at% across the length of the grain. The blocky grains do not appear to be associated with a specific plateau of oxygen content.

In the post transition sample, a very small (~ 10 nm wide) plateau is observed at around 40 at%. This corresponds to the width of the intermediate layer observed in this sample. There is no plateau at 30 at%, as the oxygen content decreases quickly in the metal.

The transition affects the structure of the oxide/metal interface: all the oxygen-rich layers (containing between 66 at% (oxide) and 29 at% (solid solubility limit of O in Zr)) tend to disappear at transition, likely to start being formed slowly again afterwards. An explanation for this phenomenon is that oxide is formed faster right after transition, and a large amount of oxygen is necessary to maintain the fast growth rate. This could consume the oxygen-rich layers previously present ahead of the slow growing oxide, resulting in the disappearance of both the intermediate layer (ZrO phases) and the suboxide (ω-Zr).

The ensemble of these observations is self-consistent, in good agreement with previous observations and with results yielded by different techniques. Some more work is necessary to fully characterize the interface and the transition process.

V. CONCLUSIONS

A detailed transmission electron microscopy study using FIB-prepared samples was conducted to characterize the structures of oxides formed in Zircaloy-4 and study the causes and consequences of the kinetic

transition on the microstructure. The main conclusions are as follows:

- The oxide layer is composed of both equiaxed and columnar grains. The equiaxed grains are found near cracks, near the oxide water interface, and in regions oxidized during the kinetic transition happened. A higher content of tetragonal ZrO_2 is often found in these regions. In the bulk of the oxide, both monoclinic and tetragonal reflections are observed in electron diffraction patterns, with the tetragonal oxide normally associated with small equiaxed grains.

- The monoclinic oxide texture evolves within the oxide layer: at the oxide/metal interface, some of the reflections are diffuse, while further from the interface, a more marked texture with $(200)_M$ planes poles aligned close to the oxide growth direction is observed. However, the microtexture is not as marked: when tilting the sample, each grain responds differently as a result of strong grain to grain misorientation.

- The $Zr(Cr,Fe)_2$ precipitates are incorporated into the oxide in metallic form and later become oxidized. Oxidized precipitates are observed as round regions containing very small grains with extensive cracks. Those grains are identified by diffraction pattern to be mainly tetragonal. EFTEM mapping shows high content of Fe and Cr in the SPP and the matrix surrounding it.

- Three different features at the oxide/metal interface are seen in the pre-transition oxide: (i) a small intermediate layer, associated with a ZrO phase by its oxygen content (between 45 and 55 at%); (ii) blocky grains found at some places along the interface, with diffraction patterns indexed as Zr_3O; (iii) an oxygen-saturated suboxide layer in the metal (30 O at%), identified as ω-Zr.

- With the exception of the intermediate layer, these interfacial regions are not observed after transition. The intermediate layer is smaller than before transition (10 nm, compared to 50nm). The high corrosion rates at transition consume these layers, which start to develop again as the corrosion rate falls in the post transition regime.

ACKNOWLEDGMENTS

The authors would like to thank Ke Wang and Trevor Clark for their precious help and advices regarding the TEM at Penn State. This work has been made possible thanks to the variety of samples oxidized by Westinghouse, as part of the MUZIC2 program.

REFERENCES

1. Yilmazbayhan, A. et al., “TEM Examination of Oxide Layers Formed in Zr Alloys”. *Journal of Nuclear Materials*, **349**, pp. 265 -281 (2006)
2. Bechade, J.L. et al., “Studies of Zirconium Alloy Oxide Layers Using Synchrotron Radiation”. *Materials Science Forum*, **347**, pp. 471-476 (2000)
3. Yilmazbayhan, A. et al., “Structure of Zirconium Alloy Oxides formed in pure water studied with Synchrotron radiation and optical microscopy: relation to corrosion rate”. *Journal of Nuclear Materials*, **324**, pp. 6-22 (2004)
4. Pêcheur, D. et al., "Precipitate Evolution in the Zircaloy-4 Oxide Layer". *Journal of Nuclear Materials*, **189**, pp. 318-332 (1992)
5. lltis, X. and Michel, H., "Transmission Electron Microscopy Study of a Locally Ordered Zr-O Solid Solution Obtained by an Oxidation Treatment of a Zircaloy-4 Alloy". *Journal of Alloys and Compounds*, **177**, pp. 71-82 (1991)
6. Dong, Y. et al, “Atom Probe Tomography study of Alloying element distributions in Zr alloys and their oxides”. *Journal of Nuclear Materials*, to be submitted (2013)
7. Motta, A.T. et al, “Microstructural Characterization of Oxides Formed on Model Zr Alloys Using Synchrotron Radiation”.15th International Symposium on Zirconium in the Nuclear Industry, *ASTM STP 1505*, pp. 486-506 (2009)
8. Cox, B. and Pemsler, J.P., “Diffusion of Oxygen in Growing Zirconia Films”. *Journal of Nuclear Materials*, **28**, p. 73-78 (1968)
9. Foord, D.T. and Newcomb, S.B., "The microstructural characterisation of factors which determine the degradation behaviour of Zircaloy-4". Third International Conference on the Microscopy of Oxidation, *The Institute of Materials, London, UK*, pp. 488-499 (1997)
10. Furuta, K. and Motohashi, H., "Products at the surface of Zircaloy cladding under LOCA conditions". *Journal of Nuclear Materials*, **95**(3), pp. 303-306 (1980)
11. Hutchinson, B. et al., “A study of the structure and chemistry in Zircaloy-2 and the resulting oxide after high temperature corrosion”. 15th International Symposium on Zirconium in the Nuclear Industry, *ASTM STP 1505*, pp. 269-284 (2009)
12. Hudson, D. et al., “Zirconium oxidation on the atomic scale”. *Ultramicroscopy*, **5**, pp. 667-671 (2009)